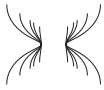
JGSP **52** (2019) 67–102

JOURNAL OF
Geometry and Symmetry in Physics
ISSN 1312-5192

SOME CLASSES OF SHAPES OF THE ROTATING LIQUID DROP

VLADIMIR I. PULOV AND IVAÏLO M. MLADENOV

Presented by Ivaïlo Mladenov

Abstract. The problem of a fluid body rotating with a constant angular velocity and subjected to uniform external pressure is of real interest in both fluid dynamics and nuclear theory. Besides, from the geometrical viewpoint the sought equilibrium configuration of such system turns out to be equivalent to the problem of determining the surface of revolution with a prescribed mean curvature. In the simply connected case, the equilibrium surface can be parameterized explicitly via elliptic integrals of the first and second kind.

MSC: 53A04, 53A05, 53A10, 53B50, 33E05, 53C22, 76B45, 76D45
Keywords: Axially symmetric surfaces, capillarity, Jacobian elliptic functions, elliptic integrals, fluid dynamics, geodesics, parameterizations, surface geometry

Contents

doi: 10.7546/jgsp-52-2019-67-102

List of Symbols

(OX, OY, OZ)	Cartesian coordinate system in $\mathbb{R}^3$
(x, y, z)	Cartesian coordinates
$\mathcal{S}$	surface in the three-dimensional space
$(x(u,v), y(u,v), z(u,v))$	parameterization of the surface $\mathcal{S}$
(OX, OZ)	Cartesian coordinate system in $\mathbb{R}^2$
(x, z)	Cartesian coordinates in the plane
$(x_j(u), z_j(u))$	parameterization of the profile curves of the shapes from j-th class
$\tilde{a}, \tilde{c}$	physical constants
a	dimensionless angular velocity
$\nu \in \mathbb{R}$	shape parameter
N, S	North and South Poles of closed surfaces
E	Equator
κ_μ, κ_π	meridional and parallel curvatures
$\mathcal{R}_\mu, \mathcal{R}_\pi$	meridional and parallel radii
r	radius of the equator
$\mathring{\kappa}_\mu, \mathring{\kappa}_\pi$	equatorial principal curvatures
$P(t)$	quadratic polynomial
$\mathcal{D}$	discriminant of $P(t)$
σ, τ	roots of $P(t)$
σ_j, τ_j	roots of $P(t)$ related to the shapes of the j-th class
θ	angular coordinate of the parallel circle
ϕ	angular coordinate of the meridians
$\mathbf{n}, \mathbf{n}_\theta, \mathbf{n}_\phi$	unit vectors along the normal, meridional and parallel directions
k	modulus of the elliptic function
k_j	modulus of the elliptic function related to the shapes of class j
$\mathrm{am}(u,k)$	Jacobian amplitude function
$\Delta(\varphi) = \sqrt{1 - k^2 \sin^2\varphi}$	delta function
$\mathrm{sn}(u,k), \mathrm{cn}(u,k), \mathrm{dn}(u,k)$	Jacobian elliptic functions
$\mathrm{sn}^{-1}(u,k), \mathrm{cn}^{-1}(u,k), \mathrm{dn}^{-1}(u,k)$	inverse Jacobian elliptic functions
$F(\varphi,k), E(\varphi,k)$	elliptic integrals of the first and second kind
$K(k), E(k)$	complete elliptic integrals of the first and second kind
$\Pi(\varphi,n,k), \Pi(n,k)$	incomplete and complete elliptic integrals of the third kind

1. Introduction

Dynamics, and respective analyses of a rotating liquid drop held together by the surface tension were initiated long time ago by Plateau [18]. In his experiments he considers a fluid body with incompressible mass rotating with a constant angular velocity and subjected to surface tension. The problem then is to find the shape which this mass will have under prescribed angular velocity.

The only force acting inside the drop is the centrifugal force generated from the potential $\frac{\rho\omega^2\mathcal{R}^2}{2}$ and directed away from the axis. Here, ρ is the difference between the densities ρ_i of the inner and ρ_e of the exterior mediums, ω is the fixed angular velocity and $\mathcal{R}$ is the radial distance from the axis of rotation. Because the fluid is assumed to be incompressible, a constant internal pressure p_i results within the body. According to the Laplace-Young equation [10, 15], at the free surface $\mathcal{S}$ enclosing the drop the surface tension σ generates a pressure proportional to its mean curvature H, $\sigma\, H$. Finally, we must also add the constant pressure p_e of the external fluid. The surface in equilibrium is therefore described by equating these pressures

$$p_i + \frac{\rho\omega^2\mathcal{R}^2}{2} = \sigma H + p_e \tag{1}$$

where $\omega, p_e, p_i, \rho, \sigma$ are constants. This then reduces immediately to the equation

$$H = 2\tilde{a}\mathcal{R}^2 + \tilde{c} \tag{2}$$

where the constants

$$\tilde{a} = \frac{\rho\omega^2}{4\sigma}, \qquad \tilde{c} = \frac{p}{\sigma} \tag{3}$$

allow arbitrary values $\tilde{a}, \tilde{c} \in \mathbb{R}$. Note that the signs of $\tilde{a}$ and $\tilde{c}$ are determined by the signs of the differences of the densities $\rho = \rho_i - \rho_e$ and the pressures $p = p_i - p_e$ in the vicinity of the two sides of the interface between the two fluids.

As it was shown by Rayleigh [21] and exploited later by others (see e.g. [4] and [14]) the shape of the rotating liquid drop depends only on one parameter which is the non-dimensional angular velocity (rotation rate)

$$a = \frac{\rho\omega^2 r^3}{4\sigma} \tag{4}$$

where r is the equatorial radius of the drop (see Fig. 3). The dimensionless rotation rate a (denoted elsewhere [21] as Ω, or by Σ in [4] and [14]) is actually the normalized parameter $\tilde{a}$ with the normalizing factor r^3 (cf. also [13] and Table 1).

Quite often in the literature, including the aforementioned articles, the rotation rate appears with a denominator 8σ which is two times bigger than the denominator of a as it is defined in (4). This however does not change the value of a which is due to the use of a different convention for the determination of the surface tension σ leading to twice as smaller values than the values of σ used in (4).

In view of our further investigation of the possible shapes of the rotating liquid drop we prefer to use, instead of the physical quantity a, a parameter with a clear geometric meaning. We define

$$\nu = \frac{\mathring{\kappa}_\mu}{\mathring{\kappa}_\pi} = r\,\mathring{\kappa}_\mu \tag{5}$$

where $\mathring{\kappa}_\mu = \kappa_\mu(\pi/2)$ and $\mathring{\kappa}_\pi = \kappa_\pi(\pi/2) = 1/r$ are the meridional and the parallel principal curvatures respectively, that are calculated along the equator E, i.e., for $\mathring{\theta} = \pi/2$ (cf. Fig. 1 – Fig. 3 and the assumptions made in Section 2).

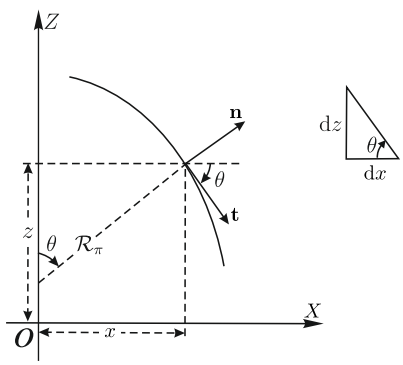

Figure 1. Geometry of the profile curve.

By substituting in (2) with $\mathcal{R} \equiv r$ and making use of the mean curvature of the drop's surface at the points of the equator $\mathring{H} = (\mathring{\kappa}_\mu + \mathring{\kappa}_\pi)/2$ one immediately arrives at the relations

$$\tilde{a} = \frac{a}{r^3}, \qquad \tilde{c} = \frac{\nu+1}{2r} - \frac{2a}{r}. \tag{6}$$

As a result the initially given physical quantities $\tilde{a}$ and $\tilde{c}$ have been expressed through two dimensionless parameters a and ν and a parameter r with the dimension of length. In the next section we derive formula for the dimensionless angular velocity a in terms of the geometric parameters r and ν. Eventually, this allows us to leave the physical description and continue our study of the rotating liquid drop from the viewpoint of the geometry of plane curves [2, 3, 9, 10, 17, 19, 20].

2. Geometry: Preliminaries

Let the surface $\mathcal{S}$ under consideration, which is the drop itself, is generated by the rotation of a plane curve γ (profile curve) about the OZ-axis of some orthogonal (OX, OY, OZ) coordinate system in $\mathbb{R}^3$. We assume that $\mathcal{S}$ intersects the XOY-plane at right angle $\mathring{\theta} = \pi/2$ and the profile curve γ lies in the XOZ-plane where $\mathcal{R}$ coincides with the Cartesian coordinate x. Let this curve γ is specified by the function $z = z(x)$, $x \geq 0$, which is chosen in such a way that $z(r) = 0$ for some positive number r (see Fig. 3). The curve on the surface traced by this point (i.e., the point $(r, 0)$ of the profile curve) is the *equator* of $\mathcal{S}$ for which we assume that it has a predetermined (fixed) radius r.

Let us now recall the well-known fundamental relations among meridional curvature κ_μ, circumferential curvature κ_π and the mean curvature H for surfaces of revolution [15]

$$\kappa_\mu = \frac{\mathrm{d}(x\kappa_\pi)}{\mathrm{d}x}, \qquad H = \frac{\kappa_\mu + \kappa_\pi}{2}. \tag{7}$$

The simultaneous solution of the system of equations (2) and (7) for $\mathcal{R} \equiv x$ is

$$\kappa_\pi = \tilde{a}x^2 + \tilde{c} + \frac{C}{x^2}, \qquad \kappa_\mu = 3\tilde{a}x^2 + \tilde{c} - \frac{C}{x^2} \tag{8}$$

where C is an integration constant which is assumed further on to be zero $C \equiv 0$. We make this assumption here in order to get analytical formulas for the rotating drop. At the moment, letting C to be non-zero (despite that this is the most interesting case) can be accessed only numerically [5].

Moreover, if $\mathcal{R}_\pi$ is the distance from the surface point to the intersection of the normal at that point with the symmetry axis (Fig. 1), meaning that $\mathcal{R}_\pi$ is the radius of the parallel principal curvature, then we have additionally

$$\kappa_\pi = \frac{1}{\mathcal{R}_\pi} = \frac{\sin\theta}{x} \tag{9}$$

and therefore

$$\frac{\mathrm{d}z}{\mathrm{d}x} = \pm\tan\theta = \pm\frac{x\kappa_\pi}{\sqrt{1-(x\kappa_\pi)^2}}. \tag{10}$$

Finally, the ordinate of the profile curve is given by the integral

$$z(x) = \pm\int \frac{(\tilde{a}x^3 + \tilde{c}x)\mathrm{d}x}{\sqrt{1-(\tilde{a}x^3+\tilde{c}x)^2}}. \tag{11}$$

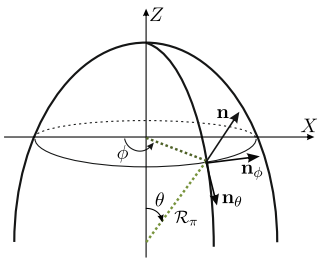

Figure 2. A sketch of a typical surface of revolution.

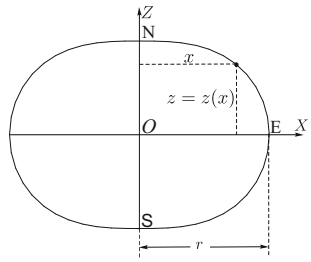

Figure 3. A typical closed profile curve in XOZ-plane.

Here, the indefinite integral produces an expression in x that gives the x-dependent formula for z. From these considerations, we obtain a profile curve for the rotating drop, $(x, z(x))$ with

$$\mathbf{x}(u, v) = (x\ \cos(v), x\ \sin(v), z(x))$$

being a parametrization for the surface of revolution $\mathcal{S}$ that embraces the drop.

Returning back to the equations (8) we see at once that the shapes we have to deal with are in fact *linear Weingarten surfaces* (cf [7, 8, 11, 12] obeying the relation (if $C = 0$)

$$\kappa_\mu = 3\kappa_\pi - 2\tilde{c} \tag{12}$$

which can be equivalently written as

$$\kappa_\mu = 3\kappa_\pi + \frac{\nu - 3}{r} \tag{13}$$

where

$$\tilde{c} = \frac{1 - a}{r}, \qquad a = \frac{\nu - 1}{2}\cdot \tag{14}$$

The latter is a direct consequence of equation (12) after substitution of $\tilde{c}$ from (6) and calculating at the points of the equator. For ease of the reader we have collected in Table 1 the most important relationships between various parameters that have been used in the literature on the subject.

Three particular surfaces can be immediately recognized: the right circular cylinder for $\nu = 0$, the sphere for $\nu = 1$ (both having the same constant parallel curvatures, i.e., $\kappa_\pi(\theta) \equiv 1/r$, $\theta \in [-\pi/2, \pi/2]$), and the rotational surface associated with $\nu = 3$ which is known as *LW*(2) *balloon* [19] (cf also Table 2).

Except the three surfaces – the sphere, the right circular cylinder and the surface obtained for $\nu = 9$ (see below), that are parameterizable by elementary functions,

Table 1. Important relationships between the basic parameters.

<table>
<tr><td>$\tilde{a}=\dfrac{\rho\omega^2}{4\sigma}$</td><td>$\tilde{c}=\dfrac{p}{\sigma}$</td><td rowspan="2">$a=r^3\tilde{a}$
$c=r\tilde{c}$
Ω [21] $\equiv \Sigma$ [4, 14] $\equiv a$ [13]</td></tr>
<tr><td>$a=\dfrac{\rho\omega^2 r^3}{4\sigma}$</td><td>$c=\dfrac{pr}{\sigma}$</td></tr>
<tr><td colspan="2">$\nu=\dfrac{\mathring{\kappa}_\mu}{\mathring{\kappa}_\pi}=r\mathring{\kappa}_\mu$</td><td>$r$ is the equatorial radius
$\mathring{\kappa}_\pi, \mathring{\kappa}_\mu$ are the principal curvatures</td></tr>
<tr><td>$\tilde{a}=\dfrac{\nu-1}{2r^3}$
$\nu=2\tilde{a}r^3+1$</td><td>$\tilde{c}=\dfrac{3-\nu}{2r}$
$\nu=3-2\tilde{c}r$</td><td rowspan="2">$\tilde{a}r^3+\tilde{c}r=1$
$a+c=1$
$\rho\omega^2r^3+4pr=4\sigma$
$\rho\omega^2r^3=2(\nu-1)\sigma$
$2pr=(3-\nu)\sigma$</td></tr>
<tr><td>$a=\dfrac{\nu-1}{2}$
$\nu=2a+1$</td><td>$c=\dfrac{3-\nu}{2}$
$\nu=3-2c$</td></tr>
</table>

the condition (12) defines surfaces which can not be described in the same way. One such surface is the above mentioned *LW*(2) balloon. The *LW*(2) balloon satisfies the relation $\kappa_\mu = 3\kappa_\pi$, and therefore belongs to the special class of linear Weingarten *LW*(*n*) *surfaces* (for relevant definitions and details see [19]).
Further, by substituting in the integral (11) the expressions for $\tilde{a}$ and $\tilde{c}$, given by the equations (6) and (14), the profile curve (the upper right branch) of the rotating liquid drop takes the form

$$z(\chi) = \pm\, r \int_{\chi}^{1} \frac{((\nu-1)t-\nu+3)\mathrm{d}t}{\sqrt{(1-t)\left((\nu-1)^2t^2-(\nu-1)(\nu-5)t+4\right)}}, \qquad \chi=\frac{x^2}{r^2} \tag{15}$$

in which for the surfaces lying inside the cylinder $\nu = 0$

$$x \in [0, r], \qquad \chi \in [0, 1], \qquad t \in (0, 1) \tag{16}$$

and for the surfaces positioned outside the cylinder

$$x \in [r, +\infty), \qquad \chi \in [1, +\infty), \qquad t \in (1, +\infty). \tag{17}$$

For $\nu = 1$ and $\nu = 9$ the integral (15) can be evaluated only in terms of elementary functions as these are the cases when the quadratic polynomial under the radical

$$P(t) = (\nu-1)^2t^2-(\nu-1)(\nu-5)t+4, \qquad \nu \neq 1 \tag{18}$$

is either reduced to constant or has multiple roots so that two surfaces are immediately obtained: the sphere for $\nu = 1$, and the surface for $\nu = 9$ which generating curve $\gamma(x) = (x, 0, z(x))$, $x \in (r/2, r]$ is given by the formula

$$\gamma(u) = \Big(r\sin u,\ 0,\ r\Big(\frac{1}{\sqrt{3}}\arctan\frac{2\cos u}{\sqrt{3}} - \cos u\Big)\Big), \quad u \in (\pi/6, 5\pi/6]\,. \quad (19)$$

A collection of shapes with known values for the shape parameter ν (resp. a) are given in Table 2. The next Table 3 contains lists of explicit expressions representing the mean and the principal curvatures of the drop's shape in relationship with different selections of shape parameters.

Table 2. Some particular shapes and the corresponding values of the parameters ν and a.

Shapes	ν	a
right circular cylinder	0	-0.5
sphere	1	0
$LW(2)$	3	1
biconcave discoid with one contact point	5.6582	2.3291
shape parameterized via elementary functions	9	4

When ν is not equal to one or nine the above integral belongs to the class of non-elementary *elliptic integrals*. Our present goal is to build up the canonical forms of the elliptic integral (15) for all values of the parameter $\nu \in (-\infty, +\infty)$.

3. Elliptic Integrals and Functions

As it was first shown by Legendre (1811-1819), the elliptic integrals are always reducible to their *canonical form*, which means that they are expressible as a linear combination of elementary functions and the three fundamental elliptic integrals – the so called *normal elliptic integrals* of the first

$$F(\varphi,k)\equiv\int\limits_0^{\zeta}\frac{\mathrm{d}t}{\sqrt{(1-t^2)(1-k^2t^2)}}=\int\limits_0^{\varphi}\frac{\mathrm{d}\theta}{\sqrt{1-k^2\sin^2\theta}} \tag{20}$$

second

$$E(\varphi,k)\equiv\int\limits_0^{\zeta}\sqrt{\frac{1-k^2t^2}{1-t^2}}\mathrm{d}t=\int\limits_0^{\varphi}\sqrt{1-k^2\sin^2\theta}\,\mathrm{d}\theta \tag{21}$$

and respectively the third kind

$$\Pi(\varphi,n,k)\equiv\int\limits_0^{\zeta}\frac{\mathrm{d}t}{(1-nt^2)\sqrt{(1-t^2)(1-k^2t^2)}}=\int\limits_0^{\varphi}\frac{\mathrm{d}\theta}{(1-n\sin^2\theta)\sqrt{1-k^2\sin^2\theta}}\cdot \tag{22}$$

These three standard elliptic integrals depend on the variable upper limit ζ or φ, which is considered as their *argument*

$$\zeta=\sin\varphi,\qquad \zeta\in(0,1],\qquad \varphi\in(0,\frac{\pi}{2}]$$

and the so called *elliptic modulus* $k\in(0,1)$, while the third one depends on one additional *parameter* which is assumed to be different from one and k^2 (for more details about the elliptic integrals, see e.g. [1]).

In order to reduce the elliptic integral (15) to its canonical form we will make substitutions involving Jacobian elliptic functions. The method dates back to Abel

Table 3. Mean and principal curvatures expressed via different combinations of parameters ($\mathcal{R}$ – radial distance from the axis of revolution).

Parameters	Mean curvature	Principal curvatures	Weingarten relation
$\tilde{a},\,\tilde{c}$	$H=2\tilde{a}\mathcal{R}^2+\tilde{c}$	$\kappa_\pi=\tilde{a}\mathcal{R}^2+\tilde{c}$ $\kappa_\mu=3\tilde{a}\mathcal{R}^2+\tilde{c}$	$\kappa_\mu=3\kappa_\pi-2\tilde{c}$
$a,\,c,\,r$	$H=\frac{2a}{r^3}\mathcal{R}^2+\frac{c}{r}$	$\kappa_\pi=\frac{a}{r^3}\mathcal{R}^2+\frac{c}{r}$ $\kappa_\mu=\frac{3a}{r^3}\mathcal{R}^2+\frac{c}{r}$	$\kappa_\mu=3\kappa_\pi-\frac{2c}{r}$
$r,\,\nu$	$H=\frac{\nu-1}{r^3}\mathcal{R}^2+\frac{3-\nu}{2r}$	$\kappa_\pi=\frac{\nu-1}{2r^3}\mathcal{R}^2+\frac{3-\nu}{2r}$ $\kappa_\mu=\frac{3(\nu-1)}{2r^3}\mathcal{R}^2+\frac{3-\nu}{2r}$	$\kappa_\mu=3\kappa_\pi+\frac{\nu-3}{2r}$

(1827-1828) and Jacobi (1828) who almost simultaneously suggested to consider the inversion of the integrals

$$u = F(\varphi, k) \equiv \int_0^{\zeta} \frac{\mathrm{d}t}{\sqrt{(1-t^2)(1-k^2t^2)}} = \int_0^{\varphi} \frac{\mathrm{d}\theta}{\sqrt{1-k^2\sin^2\theta}}$$

as new functions which are called am (*amplitude*) and respectively sn (*sine amplitude*)

$$\varphi = \mathrm{am}(u,k), \qquad \zeta = \sin\varphi = \mathrm{sn}(u,k). \tag{23}$$

Two related functions namely, cn (*cosine amplitude*) and dn (*delta amplitude*) were introduced via the formulas

$$\Delta\varphi = \sqrt{1-k^2\sin^2\varphi}, \quad \mathrm{cn}(u,k) = \sqrt{1-\zeta^2} = \cos\varphi, \quad \mathrm{dn}(u,k) = \sqrt{1-k^2\zeta^2}. \tag{24}$$

The functions $\mathrm{sn}(u,k)$, $\mathrm{cn}(u,k)$ and $\mathrm{dn}(u,k)$ are called *Jacobian elliptic functions*. Their modern notation is due to Gudermann (1838). Assuming the modulus k to be fixed we will simply write $\varphi = \mathrm{am}\, u$, etc. We find it useful to visualize the composite functions by commutative "barred arrow diagrams" as the one displayed in Fig. 4.

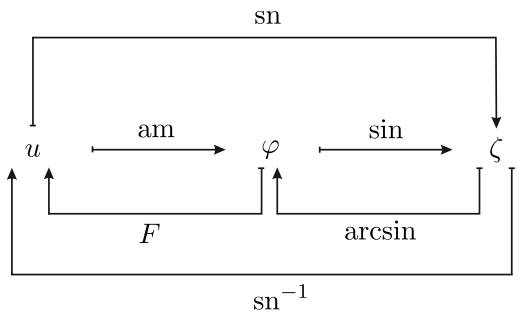

Figure 4. Commutative diagram for the inversion of the normal elliptic integral of the first kind.

As a consequence of the above formulas the following fundamental relations between the Jacobian elliptic functions are obtained

$$\mathrm{sn}^2u + \mathrm{cn}^2u = 1, \qquad \mathrm{dn}^2u + k^2\mathrm{sn}^2u = 1, \qquad \mathrm{dn}^2u - k^2\mathrm{cn}^2u = 1 - k^2 \tag{25}$$

and the representations of the normal elliptic integrals via the amplitude function or the Jacobian elliptic functions are easily revealed

$$\begin{aligned} F(\varphi,k) &= F(\mathrm{am}\,u,k) \equiv u = \int\limits_0^u \mathrm{d}\tilde{u} \\ E(\varphi,k) &= E(\mathrm{am}\,u,k) = \int\limits_0^u \mathrm{dn}^2\tilde{u}\mathrm{d}\tilde{u} \\ \Pi(\varphi,n,k) &= \Pi(\mathrm{am}\,u,n,k) = \int\limits_0^u \frac{\mathrm{d}\tilde{u}}{1-n\mathrm{sn}^2\tilde{u}}. \end{aligned} \tag{26}$$

The derivatives of the Jacobian elliptic functions with respect to their argument are obtained directly from the definitions of the respective functions

$$\frac{\mathrm{d}}{\mathrm{d}u}(\mathrm{sn}\,u) = \mathrm{cn}\,u\,\mathrm{dn}\,u, \quad \frac{\mathrm{d}}{\mathrm{d}u}(\mathrm{cn}\,u) = -\mathrm{sn}\,u\,\mathrm{dn}\,u, \quad \frac{\mathrm{d}}{\mathrm{d}u}(\mathrm{dn}\,u) = -k^2\mathrm{sn}\,u\,\mathrm{cn}\,u.$$

Let us also notice that in the case of $\zeta = 1$, respectively $\varphi = \pi/2$, the integrals (20) – (22) are said to be the *complete elliptic integrals* of the respective kind which are denoted as

$$K(k) = F(\pi/2,k), \quad E(k) = E(\pi/2,k), \quad \Pi(n,k) = \Pi(\pi/2,n,k). \tag{27}$$

In order to proceed with the canonization of the integral (15), we need to know the roots of the quadratic polynomial (18), and in what order the roots, when they are real, are related to each other and the number one, which is the third root of the polynomial under the radical $\sqrt{(1-t)P(t)}$. Depending on the sign of the discriminant

$$\mathcal{D} = (\nu-1)^3(\nu-9)$$

the roots of $P(t)$

$$\sigma = \frac{\nu-5+\sqrt{(\nu-1)(\nu-9)}}{2(\nu-1)}, \qquad \tau = \frac{\nu-5-\sqrt{(\nu-1)(\nu-9)}}{2(\nu-1)} \tag{28}$$

may be either real, for $\nu \in (-\infty,1) \cup [9,+\infty)$ or complex, for $\nu \in (1,9)$. The real roots are positive numbers, $\sigma > 0$, $\tau > 0$, and when $\sigma \neq \tau$ (simple roots), either $\sigma < \tau$, for $\nu \in (-\infty,1)$, or $\tau < \sigma$, for $\nu \in (9,+\infty)$.

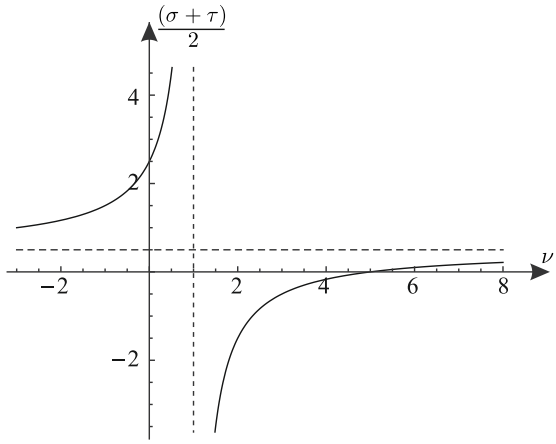

Figure 5. Graphic of the arithmetic mean of the roots of the polynomial $P(t)$ versus ν and the dashed lines are the asymptotes of the function.

A more precise reasoning reveals that in the case of simple roots there are exactly three possibilities for the number one: to be the smallest $1 < \tau < \sigma$, the largest $\sigma < \tau < 1$, or between the other two, i.e., $\sigma < 1 < \tau$. All of the above statements can be proven by inspection relying on the arithmetic mean of the roots σ and τ versus ν

$$\frac{1}{2}(\sigma+\tau) = \frac{\nu-5}{2(\nu-1)}$$

and the observation that the sign of $P(1) = 4\,\nu$ alternates while $P(0) = 4$ is always positive (cf. the graphic in Fig. 5). Consequently, there are four specific ranges of the values of the parameter ν, related to the four possible ranges of the roots of the polynomial under the radical $\sqrt{(1-t)P(t)}$

$$\begin{array}{ll} \mathcal{S}^{\mathrm{I}}(\nu) & \nu \in (-\infty, 0), \qquad 0 < \sigma_1 < 1 < \tau_1 \\ \mathcal{S}^{\mathrm{II}}(\nu) & \nu \in (0, 1), \qquad 1 < \sigma_2 < \tau_2 \\ \mathcal{S}^{\mathrm{III}}(\nu) & \nu \in (1, 9), \qquad \sigma_3 \in \mathbb{C},\ \tau_3 \in \mathbb{C} \\ \mathcal{S}^{\mathrm{IV}}(\nu) & \nu \in (9, +\infty), \qquad 0 < \tau_4 < \sigma_4 < 1. \end{array} \tag{29}$$

As a result the whole set of shapes is splitted into four *classes of surfaces* $\mathcal{S}^{\mathrm{I}}(\nu)$ - $\mathcal{S}^{\mathrm{IV}}(\nu)$ which differ by the range of the values of the parameter ν (cf. Fig. 6). Our next goal is to present the canonical parameterizations of these surfaces in each one of these classes by using the normal forms of the elliptic integrals and the Jacobian elliptic functions. We start with some observations regarding the general properties of the considered shapes. In order that the integral (15) is well defined

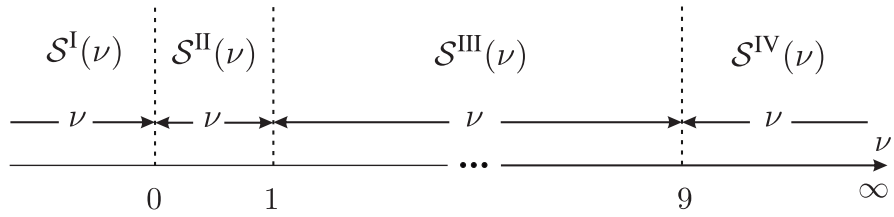

Figure 6. Ranges of the variable ν related to the different classes of shapes of the rotating liquid drop.

it is necessary that the polynomial $P(t)$ obey to some constraints. In the range of integration (16), i.e., for the surfaces lying inside the cylinder, the values of the polynomial have to be positive

$$P(t) > 0, \qquad t \in (0, 1)$$

and in the range of integration (17), i.e., for the surfaces that are outside the cylinder, the values of the polynomial have to be negative

$$P(t) < 0, \qquad t \in (1, +\infty).$$

Under such constraints, as it is easily seen from the suggestive graphics in Fig. 7, it follows that the first and the fourth classes of shapes consist of open surfaces, lying either outside the cylinder

$$\mathcal{S}^{\mathrm{I}}(\nu): \qquad x \in [r, r\sqrt{\tau_1}], \qquad \chi \in [1, \tau_1], \qquad t \in (1, \tau_1) \tag{30}$$

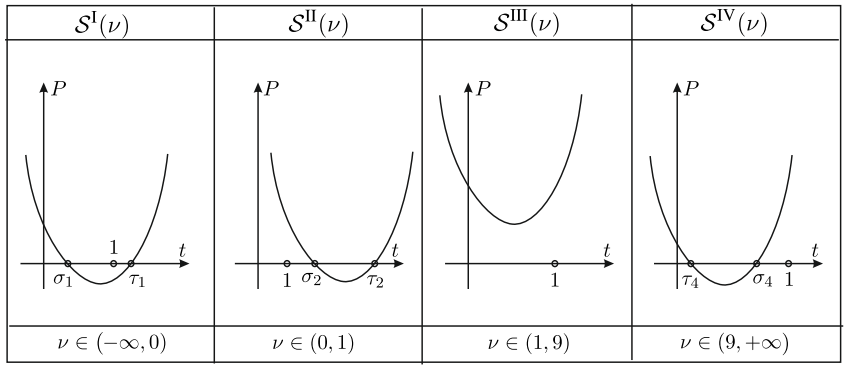

Figure 7. Graphics of the polynomial $P(t)$ related to the different classes of shapes of the rotating liquid drop.

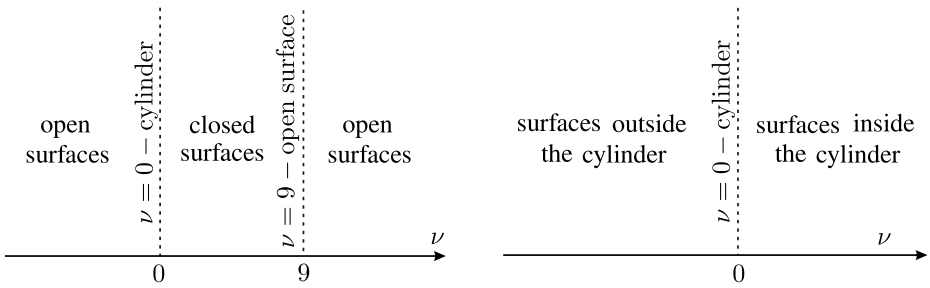

Figure 8. Ranges of the variable ν related to open and closed surfaces (left), and that ones lying outside and inside the cylinder (right).

or inside the cylinder

$$\mathcal{S}^{\mathrm{IV}}(\nu): \qquad x \in [r\sqrt{\sigma_4}, r], \qquad \chi \in [\sigma_4, 1], \qquad t \in (\sigma_4, 1). \tag{31}$$

All of the surfaces belonging to the classes $\mathcal{S}^{\mathrm{II}}(\nu)$ and $\mathcal{S}^{\mathrm{III}}(\nu)$ are closed and they are lying inside the cylinder, i.e.,

$$\mathcal{S}^{\mathrm{II}}(\nu) \text{ and } \mathcal{S}^{\mathrm{III}}(\nu): \qquad x \in [0, r], \qquad \chi \in [0, 1], \qquad t \in (0, 1). \tag{32}$$

Thus the whole set of shapes are divided into two subsets of open and closed surfaces, obtained respectively for $\nu \in (-\infty, 0] \cup [9, +\infty)$ and $\nu \in (0, 9)$, and lying either outside (for negative ν) or inside (for positive ν) of the cylinder (Fig. 8). As it will be seen below the shapes differ also on whether they have or do not

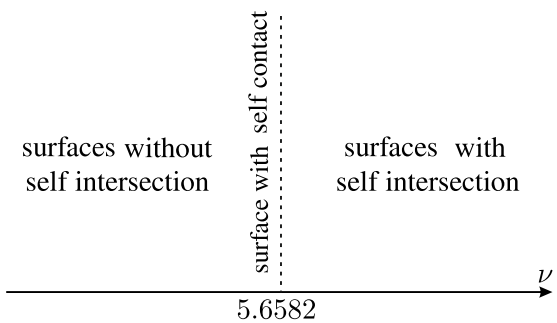

Figure 9. Ranges of the variable ν related to surfaces with and without self intersections.

have points of intersection (Fig. 9), thus splitting up into two subsets of shapes for $\nu \in (-\infty, 5.6582)$ and $\nu \in (5.6582, +\infty)$ respectively. The limiting shape generated by $\nu = 5.6582$ has a point of self contact (cf. Fig. 17 – Fig. 18). In what follows we will derive not one but three different parameterizations for each class having in mind their future applications.

4. Shapes of the First Class $\mathcal{S}^{\mathrm{I}}(\nu)$

As shown above, the shapes of the first class (for $\nu \in (-\infty, 0)$, cf. Fig. 6) are open surfaces lying outside the cylinder $\nu = 0$, whose profile curves (upper right parts), according to the equation (15) are given by the formula

$$z_1(\chi) = \frac{r}{2(1-\nu)} \int_1^{\chi} \frac{((\nu-1)t - \nu + 3)\mathrm{d}t}{\sqrt{(1-t)(t-\sigma_1)(t-\tau_1)}}, \quad \chi = \frac{x^2}{r^2}, \quad x \in [r, r\sqrt{\tau_1}] \quad (33)$$

where the roots σ_1 and τ_1, calculated by the equations (28) for $\nu \in (-\infty, 0)$, are such that the following inequalities hold (compare with the first item in (29) and (30))

$$0 < \sigma_1 < 1 < t < \tau_1, \qquad 0 < \sigma_1 < 1 \leq \chi \leq \tau_1. \quad (34)$$

In the limiting case $\nu = -\infty$ the surfaces degenerate to a circle with radius r.
On substituting with

$$t = 1 + \xi^2, \qquad \chi = 1 + \tilde{\chi}^2, \qquad \xi > 0, \qquad \tilde{\chi} \geq 0$$

the polynomial under the radical in (33) is transformed to a product of a sum and a difference of squares

$$z_1(\tilde{\chi}) = \frac{r}{1-\nu} \int_0^{\tilde{\chi}} \frac{((\nu-1)\xi^2 + 2)\mathrm{d}\xi}{\sqrt{(\tilde{\sigma}_1^2 + \xi^2)(\tilde{\tau}_1^2 - \xi^2)}} \quad (35)$$

where

$$\tilde{\sigma}_1 = \sqrt{1-\sigma_1}, \qquad \tilde{\tau}_1 = \sqrt{\tau_1 - 1}, \qquad 0 < \xi < \tilde{\tau}_1, \qquad 0 \leq \tilde{\chi} \leq \tilde{\tau}_1.$$

The above obtained integral can be split into two integrals

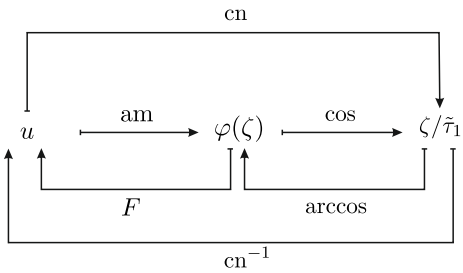

Figure 10. Commutative diagram illustrating the "inversion procedure" for the canonization of the elliptic integral (36).

$$z_1(\tilde{\chi}) = \frac{r}{1-\nu}\left(\int_0^{\tilde{\tau}_1} \frac{((\nu-1)\xi^2+2)\mathrm{d}\xi}{\sqrt{(\tilde{\sigma}_1^2+\xi^2)(\tilde{\tau}_1^2-\xi^2)}} - \int_{\tilde{\chi}}^{\tilde{\tau}_1} \frac{((\nu-1)\xi^2+2)\mathrm{d}\xi}{\sqrt{(\tilde{\sigma}_1^2+\xi^2)(\tilde{\tau}_1^2-\xi^2)}}\right)$$

each of which is obtained as a special case of the elliptic integral

$$\int_{\zeta}^{\tilde{\tau}_1} \frac{((\nu-1)\xi^2+2)\mathrm{d}\xi}{\sqrt{(\tilde{\sigma}_1^2+\xi^2)(\tilde{\tau}_1^2-\xi^2)}}, \qquad 0 \le \zeta < \tilde{\tau}_1 \tag{36}$$

with $\zeta = 0$ and $\zeta = \tilde{\chi}$, respectively. The integral (36) can be reduced to its canonical form with the help of the Jacobian cosine elliptic function, replacing ξ and ζ by the new variables $\tilde{u}$ and u

$$\xi = \tilde{\tau}_1 \mathrm{cn}(\tilde{u}, k_1), \quad \zeta = \tilde{\tau}_1 \mathrm{cn}(u, k_1), \quad u = F(\varphi(\zeta), k_1), \quad u \in (0, K(k_1)] \tag{37}$$

thereby employing the "inversion procedure" illustrated by the commutative diagram in Fig. 10 where

$$\varphi := \varphi(\zeta) = \arccos\left(\frac{\zeta}{\tilde{\tau}_1}\right), \qquad k_1 = \frac{\tilde{\tau}_1}{\sqrt{\tilde{\sigma}_1^2+\tilde{\tau}_1^2}}. \tag{38}$$

Hence, the reduction of the elliptic integral (36) follows in succession

$$\int\limits_{\zeta}^{\tilde{\tau}_1}\frac{((\nu-1)\xi^2+2)\mathrm{d}\xi}{\sqrt{(\tilde{\sigma}_1^2+\xi^2)(\tilde{\tau}_1^2-\xi^2)}}=\int\limits_{0}^{u}\frac{((\nu-1)\tilde{\tau}_1^2\,\mathrm{cn}^2\tilde{u}+2)\mathrm{dn}\,\tilde{u}\,\mathrm{d}\tilde{u}}{\sqrt{\tilde{\sigma}_1^2+\tilde{\tau}_1^2-\tilde{\tau}_1^2\,\mathrm{sn}^2\tilde{u}}}$$

$$=\frac{1}{\sqrt{\tilde{\sigma}_1^2+\tilde{\tau}_1^2}}\int\limits_{0}^{u}\frac{((\nu-1)\tilde{\tau}_1^2\,\mathrm{cn}^2\tilde{u}+2)\mathrm{dn}\,\tilde{u}\,\mathrm{d}\tilde{u}}{\sqrt{1-k_1^2\,\mathrm{sn}^2\tilde{u}}}$$

$$=\frac{1}{\sqrt{\tilde{\sigma}_1^2+\tilde{\tau}_1^2}}\Big(2\int\limits_{0}^{u}\mathrm{d}\tilde{u}+(\nu-1)\tilde{\tau}_1^2\int\limits_{0}^{u}\mathrm{cn}^2\tilde{u}\mathrm{d}\tilde{u}\Big) \tag{39}$$

$$=\frac{1}{\sqrt{\tilde{\sigma}_1^2+\tilde{\tau}_1^2}}\Big(2\int\limits_{0}^{u}\mathrm{d}\tilde{u}+\frac{(\nu-1)\tilde{\tau}_1^2}{k_1^2}\Big(\int\limits_{0}^{u}\mathrm{dn}^2\tilde{u}\mathrm{d}\tilde{u}-(1-k_1^2)\int\limits_{0}^{u}\mathrm{d}\tilde{u}\Big)\Big)$$

$$=\frac{1}{k_1^2\sqrt{\tilde{\sigma}_1^2+\tilde{\tau}_1^2}}\Big(\big(2k_1^2-(\nu-1)(1-k_1^2)\tilde{\tau}_1^2\big)F(\varphi,k_1)+(\nu-1)\tilde{\tau}_1^2E(\varphi,k_1)\Big).$$

In the above chain of equalities we have made use of the fundamental relations between the Jacobian elliptic functions (25), the normal elliptic integrals (26) – (27) and the formula for the differentiation of the Jacobian cosine function (see above in Section 3). On returning back to the profile curve (35), we make two substitutions in the last line of (39), $\zeta=0$ and $\zeta=\tilde{\chi}$, and then, by subtracting the obtained expressions, we are led to the canonical form (cf. [1, Formula (213.13)])

$$z_1(\tilde{\chi})=\frac{r}{k_1^2\sqrt{\tilde{\sigma}_1^2+\tilde{\tau}_1^2}}\Big(\Big(\frac{2k_1^2}{1-\nu}+(1-k_1^2)\tilde{\tau}_1^2\Big)\Big(K(k_1)-F(\varphi(\tilde{\chi}),k_1)\Big)$$

$$-\tilde{\tau}_1^2\Big(E(k_1)-E(\varphi(\tilde{\chi}),k_1)\Big)\Big),\quad \tilde{\chi}=\sqrt{\frac{x^2}{r^2}-1},\quad x\in[r,r\sqrt{\tau_1}]$$

where the complete elliptic integrals $K(k_1)$ and $E(k_1)$ are obtained from the incomplete ones with argument $\varphi(0)=\pi/2$ (cf. equations (27) and (38)).

Written with the help of the variable x the above expression provides the explicit parameterization of the profile curves of the surfaces from the first class in Monge representation

$$z_1(x)=\frac{r}{\sqrt{\tau_1-\sigma_1}}\Big(\big(\sigma_1-\frac{\nu-3}{\nu-1}\big)(F(\varphi,k_1)-K(k_1))+(\tau_1-\sigma_1)\big(E(\varphi,k_1)-E(k_1)\big)\Big) \tag{40}$$

$$\varphi:=\varphi(x)=\arccos\sqrt{\frac{(x/r)^2-1}{\tau_1-1}},\qquad k_1=\sqrt{\frac{\tau_1-1}{\tau_1-\sigma_1}},\qquad x\in[r,r\sqrt{\tau_1}]$$

where σ_1 and τ_1 are calculated by (28) for each one of the surfaces with a parameter $\nu \in (-\infty, 0)$. Note that the above formula describes only the upper right part of the profile curve. The whole curve is obtained by two consecutively applied reflections with respect to the coordinate axes OX and OZ (cf. Fig. 3).

The next two canonical representations of the surfaces of the first class are obtained from (40) by introducing two real parameters. One of these parameters v coincides with the angular coordinate ϕ of the meridians (Fig. 2). The other parameter u is related to $\tilde{\chi}$ (respectively to the coordinate x) in two different ways, either by the equations

$$u = \operatorname{arccsc}\sqrt{1+\tilde{\chi}^2} = \operatorname{arccsc}\left(\frac{x}{r}\right), \qquad u \in \left[\operatorname{arccsc}\sqrt{\tau_1},\ \frac{\pi}{2}\right] \tag{41}$$

or by the equations

$$u = \operatorname{cn}^{-1}\Big(\frac{\tilde{\chi}}{\tilde{\tau}_1}\Big) = \operatorname{cn}^{-1}\Big(\sqrt{\frac{(x/r)^2-1}{\tau_1-1}}\Big), \qquad u \in [0,\ 2K(k_1)]\,. \tag{42}$$

The corresponding canonical representations of the surfaces from the first class, i.e., of the surfaces obtained for $\nu \in (-\infty, 0)$, are given either by the set of equations

$$\begin{gathered}
z_1(u) = \frac{r}{\sqrt{2\delta}}\Big(\frac{2\delta+1}{2}\ (K(k_1)-F(\varphi(u),k_1)) - 2\delta(E(k_1)-E(\varphi(u),k_1))\Big) \\
\lambda_1 = \sqrt{\frac{(1-2\delta)\nu+2\delta+3}{2(1-\nu)}}, \qquad \delta = \frac{\sqrt{(\nu-1)(\nu-9)}}{2(1-\nu)} \\
k_1 = \frac{\lambda_1}{\sqrt{2\delta}}, \qquad \varphi(u) = \arccos\Big(\frac{\cot u}{\lambda_1}\Big), \quad \beta = \operatorname{arccsc}\sqrt{1+\lambda_1^2} \\
x(u,v) = r\csc u\,\cos v, \quad y(u,v) = r\csc u\,\sin v, \quad z(u,v) = z_1(u), \quad u \in \left[\beta,\ \frac{\pi}{2}\right]
\end{gathered} \tag{43}$$

or by another set of formulas in which appears the same parameter u running however in a different interval, i.e.,

$$\begin{gathered}
x_1(u) = r\sqrt{1+\lambda_1^2\operatorname{cn}^2 u}, \qquad u \in [0,\ 2K(k_1)]\,, \qquad v \in [0, 2\,\pi] \\
z_1(u) = \frac{r}{\sqrt{2\delta}}\Big(\frac{2\delta+1}{2}\Big(K(k_1)-u\Big) - 2\delta\Big(E(k_1)-E(\operatorname{am} u, k_1)\Big)\Big) \\
x(u,v) = x_1(u)\cos v, \qquad y(u,v) = x_1(u)\sin v, \qquad z(u,v) = z_1(u)
\end{gathered} \tag{44}$$

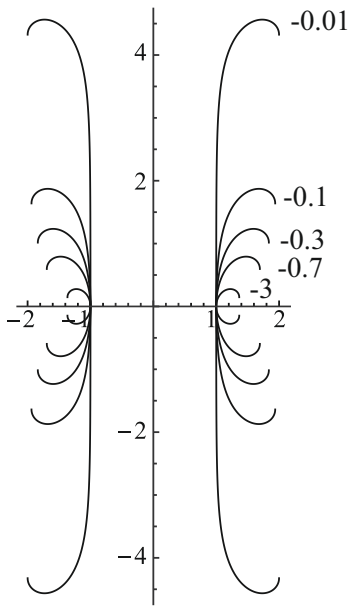

Figure 11. Some profiles of the first class.

where λ_1, k_1 and δ are defined in (43). Notice that both parameterizations rely on the same axial variable $v \in [0, 2\,\pi]$. Using one and the same notation u for parameters with different meanings and different ranges deserve some explanation. Such use allows different parameterizations to be represented in an uniformed way which generally does not lead to confusion. But nevertheless one must be careful not to confuse the parameter u in the representation (41) with the variable u that has been previously used for denoting the values of the normal elliptic integral of the first kind (cf. (26)). In the same time the variable u in the representation (42) appears in exactly that previous meaning, related here with the inverse of the Jacobian cosine function. The latter becomes at once transparent if one looks at the commutative diagram in Fig. 10 with the variable ζ replaced by $\tilde{\chi}$. It should be noted that for the parameterization (43), in the indicated interval of the parameter u, only that part of the surface $\mathcal{S}$ which is over the XOY-plane (the upper half part) can be obtained. The profile curves for both the parameterizations (43) and (44) are traced from north to south. Graphics of the profile curves of some surfaces of the first class are given in Fig. 11 for $\nu = -0.\,01, -0.\,1, -0.\,3, -0.\,7, -3$ (from outside to inside).

5. Shapes of the Second Class $\mathcal{S}^{\mathrm{II}}(\nu)$

In a contrast with the surfaces of the first class which are mainly of academic interest the shapes of the droplets in the second class are of immediate practical applications. Many years ago Vonnegut [22] has suggested a method for a measurement of the interfacial tension from the shape of the rotating drop. It is based on the experimental fact that when a fluid drop is placed in a liquid of higher density contained in a rotating horizontal tube it becomes elongated along the rotation axis until the centrifugal deformation forces are balanced by the interfacial tension.

Relying on what we have up to now it can be readily described as follows.
First, the Laplace equation in our setting can be written (using equations (7), (9) and (2)) in the form

$$\frac{\mathrm{d}\sin\theta}{\mathrm{d}x}+\frac{\sin\theta}{x}=2\,(2\tilde{a}x^2+\tilde{c}). \tag{45}$$

When $x\equiv r$, $\sin\theta\equiv 1$ and the above equality reduces to

$$4\tilde{a}r^3+2\tilde{c}\,r=1. \tag{46}$$

At the same point, the integrated form of (45) produces respectively

$$\tilde{a}r^3+\tilde{c}\,r=1. \tag{47}$$

It is easy to conclude that the only solution to the system formed by the equations (46) and (47) (taking into account that $\tilde{a}=\dfrac{\nu-1}{2r^3}$) is

$$\nu\equiv 0. \tag{48}$$

Entering with this value of the parameter ν into the general expression (15) for the

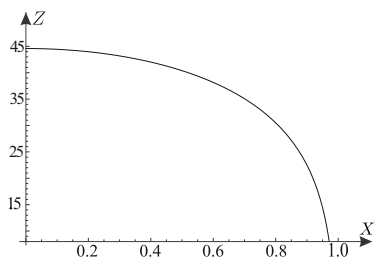

Figure 12. The shape of the rounded end of the infinitely long cylinder.

generating profile curve and forgetting for the moment about the scale we end up with the problem of evaluating the definite integral

$$z(x)=\int\limits_{\tilde{\chi}}^{1}\frac{(3-t)\mathrm{d}t}{(1-t)\sqrt{4-t}},\qquad \tilde{\chi}=x^2,\qquad x\in(0,1). \tag{49}$$

Performing the integration we find a primitive function $I(t)$ of the form

$$I(t)=-2\left(\sqrt{4-t}+\frac{\ln\dfrac{\sqrt{4-t}-\sqrt{3}}{\sqrt{4-t}+\sqrt{3}}}{\sqrt{3}}\right) \tag{50}$$

and therefore

$$z(x) = I(1) - I(\tilde{\chi}). \tag{51}$$

Because we already know that the central part of the drop is effectively an infinitely long cylinder we can omit the first (divergent) term and take into account only the second which present its rounded ends. This shape is illustrated by Fig. 12.
This case has been enlarged in [16] to more complicated surfaces which are also cylinders but this time over special curves in the horizontal plane.
As indicated in Section 3, the possible equilibrium shapes of the liquid drop of the second class (generated with $\nu \in (0, 1)$, cf. Fig. 6) are closed surfaces filling the space between the sphere $\nu = 1$ and the cylinder $\nu = 0$. According to the equation (15) and the condition (16), their profile curves (upper right parts) are given by

$$z_2(\chi) = \frac{r}{2(1-\nu)} \int_{\chi}^{1} \frac{((\nu-1)t - \nu + 3)\mathrm{d}t}{\sqrt{(1-t)(t-\sigma_2)(t-\tau_2)}}, \quad \chi = \frac{x^2}{r^2}, \quad x \in [0,\, r] \tag{52}$$

where the roots σ_2 and τ_2, calculated for $\nu \in (0, 1)$ by the equations (28), are such that the following inequalities hold (cf. the second item in (29) and (32))

$$0 < t < 1 < \sigma_2 < \tau_2, \qquad 0 \le \chi \le 1 < \sigma_2 < \tau_2. \tag{53}$$

The reduction of the above elliptic integral goes through the "inversion procedure",

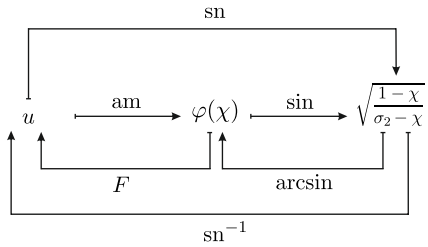

Figure 13. Commutative diagram illustrating the "inversion procedure" for the canonization of the elliptic integral (52).

as illustrated by the commutative diagram in Fig. 13, on writing

$$t = \mathrm{nc}^2(\tilde{u}, k_2) - \sigma_2 \mathrm{tn}^2(\tilde{u}, k_2), \qquad \chi = \mathrm{nc}^2(u, k_2) - \sigma_2 \mathrm{tn}^2(u, k_2) \tag{54}$$

$$u = F(\varphi(\chi), k_2), \qquad \varphi(\chi) = \arcsin\sqrt{\frac{1-\chi}{\sigma_2 - \chi}}, \qquad k_2 = \sqrt{\frac{\tau_2 - \sigma_2}{\tau_2 - 1}} \tag{55}$$

where we have used the standard notation $\mathrm{nc}\, u = 1/\mathrm{cn}\, u$ and $\mathrm{tn}\, u = \mathrm{sn}\, u/\mathrm{cn}\, u$. As a result of performing the above substitutions we arrive at the following canonical form

$$\begin{aligned} z_2(\chi) &= \frac{r}{\sqrt{\tau_2 - 1}} \int_0^u \left(\sigma_2 \mathrm{tn}^2\tilde{u} - \mathrm{nc}^2\tilde{u} + \frac{\nu - 3}{\nu - 1}\right) \mathrm{d}\tilde{u} \\ &= \frac{r}{\sqrt{\tau_2 - 1}} \left(\frac{2}{1-\nu} F(\varphi, k_2) + \frac{1-\sigma_2}{1-k_2^2}(E(\varphi, k_2) - \tan\varphi\Delta(\varphi))\right) \end{aligned} \tag{56}$$

in which the standard abbreviation $\varphi \equiv \varphi(\chi)$ has been used. The rest of the notation are as follows

$$u = \mathrm{sn}^{-1}\Big(\sqrt{\frac{1-\chi}{\sigma_2 - \chi}}\Big) = \mathrm{sn}^{-1}\Big(\sqrt{\frac{1-(x/r)^2}{\sigma_2 - (x/r)^2}}\Big), \quad u \in [-\beta,\, \beta], \quad \beta = \mathrm{sn}^{-1}(\frac{1}{\sqrt{\sigma_2}}).$$

For additional details of the reduction process, we refer the reader to the Handbook by Byrd and Friedman [1, Formulas (232.19), (313.02) and (316.02)].

On returning back to the variable x in (56) we obtain the first explicit representation of the profile curves (upper right parts) of the surfaces of the second class

$$\begin{aligned} z_2(x) &= \frac{r}{\sqrt{\tau_2 - 1}} \left(\frac{2}{1-\nu} F(\varphi, k_2) + \frac{1-\sigma_2}{1-k_2^2}(E(\varphi, k_2) - \tan\varphi\Delta(\varphi))\right) \\ \varphi &:= \varphi(x) = \arcsin\sqrt{\frac{1-(x/r)^2}{\sigma_2 - (x/r)^2}}, \qquad k_2 = \sqrt{\frac{\tau_2 - \sigma_2}{\tau_2 - 1}}, \qquad x \in [0, r] \end{aligned} \tag{57}$$

where the roots σ_2 and τ_2 are calculated by (28) for the values of the parameter ν running through the interval $(0, 1)$.

Let us now introduce a new parameter

$$u = \arcsin\sqrt{\chi} = \arcsin\left(\frac{x}{r}\right), \qquad u \in [-\frac{\pi}{2}, \frac{\pi}{2}] \tag{58}$$

which, as it can be seen from the commutative diagram in Fig. 13, should not be confused with the parameter u in equations (54) – (56).

From the above definitions it follows that the two choices of the parameter u have different relationships with the variable χ (respectively x). The corresponding canonical representations of the surfaces of the second class, i.e., of the surfaces obtained for $\nu \in (0,\, 1)$, are given either by the set of equations

$$
\begin{aligned}
z_2(u) &= r\left(\frac{2}{(1-\nu)\lambda_2}F(\varphi(u),k_2) - \lambda_2 E(\varphi(u),k_2) + \lambda_2 \tan\varphi(u)\Delta(\varphi(u))\right)\\
\varphi(u) &= \arcsin\Big(\frac{\sqrt{2(1-\nu)}\cos u}{\sqrt{2(\nu-1)\sin^2 u + (2\delta-1)\nu - 2\delta + 5}}\Big), \qquad k_2 = \frac{\sqrt{2\delta}}{\lambda_2}\\
\lambda_2 &= \sqrt{\frac{(1-2\delta)\nu + 2\delta + 3}{2(1-\nu)}}, \qquad \delta = \frac{\sqrt{(\nu-1)(\nu-9)}}{2(1-\nu)}
\end{aligned}
\tag{59}
$$

$$x(u,v) = r\,\mathrm{sn}u\,\cos v, \quad y(u,v) = r\,\mathrm{sn}u\,\sin v, \quad z(u,v) = z_2(u), \quad u\in[-\frac{\pi}{2},\frac{\pi}{2}]$$

or by another set of equations that also involve the parameter u, running however in a different range of values, i.e.,

$$
\begin{aligned}
x_2(u) &= r\sqrt{1-\mu_2^2\,\mathrm{tn}^2\,u}, \quad z_2(u) = r\Big(\frac{2u}{(1-\nu)\lambda_2} - \lambda_2 E(\mathrm{am}\,u,k_2) + \lambda_2\,\mathrm{tn}\,u\,\mathrm{dn}\,u\Big)\\
\mu_2 &= \sqrt{\frac{(1+2\delta)\nu - 2\delta + 3}{2(1-\nu)}}, \qquad \beta = \mathrm{sn}^{-1}\Big(\frac{1}{\sqrt{\mu_2^2+1}}\Big)
\end{aligned}
\tag{60}
$$

$$x(u,v) = x_2(u)\cos v, \quad y(u,v) = x_2(u)\sin v, \quad z(u,v) = z_2(u), \quad u \in [-\beta,\, \beta]$$

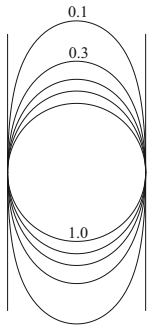

Figure 14. A few profiles from the second class.

where δ, λ_2 and the modulus k_2 are defined by the formulas in (59) and the second parameter $v \in [0, 2\,\pi]$ is the same for both parameterizations. If one makes use of the parameterization (59) in the indicated interval of the parameter u, only that part of the surface $\mathcal{S}$ which is over the XOY-plane (the upper half part) will be obtained.

The profile curves of the surface in the parameterization (59) are traced clockwise while for the parameterization (60) they are traced counterclockwise.

Fig. 14 shows various profiles drawn with parameters $\nu = 0,\ 0.1,\ 0.3,\ 0.5,\ \ 0.7$ and 1 (from outside to inside).

6. Shapes of the Third Class $\mathcal{S}^{\mathrm{III}}(\nu)$

The shapes from the third class (for $\nu \in (1, 9)$, cf. Fig. 6) are closed surfaces lying inside the sphere $\nu = 1$, which profile curves (the upper right parts) according to equations (15) – (16) are given by the formula

$$z_3(\chi) = \frac{r}{2(\nu-1)} \int\limits_{\chi}^{1} \frac{((\nu-1)t - \nu + 3)\mathrm{d}t}{\sqrt{(1-t)(t-\sigma_3)(t-\tau_3)}}, \quad \chi = \frac{x^2}{r^2}, \quad x \in [0,\, r]. \tag{61}$$

The roots σ_3 and τ_3 of the polynomial $P(t)$, calculated by the equations (28) for $\nu \in (1, 9)$, are complex numbers (compare the third item in (29) and (32)). The reduction of the above integral to normal form relies on the substitutions (cf. [1, Formula (243.00)])

$$t = \frac{1 - A + (1 + A)\mathrm{cn}(\tilde{u}, k_3)}{1 + \mathrm{cn}(\tilde{u}, k_3)}, \qquad \chi = \frac{1 - A + (1 + A)\mathrm{cn}(u, k_3)}{1 + \mathrm{cn}(u, k_3)} \tag{62}$$

where

$$A = \frac{1}{2}\sqrt{(\sigma_3 + \tau_3 - 2)^2 - (\sigma_3 - \tau_3)^2}, \qquad k_3 = \frac{1}{2}\sqrt{2 - \frac{\sigma_3 + \tau_3 - 2}{A}}. \tag{63}$$

The commutative diagram in Fig. 15 indicates the fundamental role of the "inversion procedure" in canonizing the integral (61) achieved by introducing the relations

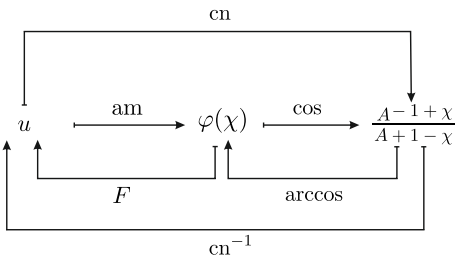

Figure 15. Commutative diagram illustrating the "inversion procedure" for the canonization of the elliptic integral (61).

$$u = F(\varphi(\chi), k_3), \qquad \varphi(\chi) = \arccos\Big(\frac{A - 1 + \chi}{A + 1 - \chi}\Big). \tag{64}$$

As a result of performing the above substitutions the following canonical form of the profile curve (61) is obtained

$$z_3(\chi) = \frac{r}{2}\Big(\Big(\sqrt{A} + \frac{2}{(\nu-1)\sqrt{A}}\Big)F(\varphi, k_3) - 2\sqrt{A}\int_0^u \frac{\mathrm{d}\tilde{u}}{1+\mathrm{cn}\tilde{u}}\Big)$$
$$= \frac{r}{2}\Big(\Big(\frac{2}{(\nu-1)\sqrt{A}} - \sqrt{A}\Big)F(\varphi, k_3) + 2\sqrt{A}\Big(E(\varphi, k_3) - \frac{\sin\varphi\Delta(\varphi)}{1+\cos\varphi}\Big)\Big) \tag{65}$$

in which $\varphi \equiv \varphi(\chi)$

$$u = \mathrm{cn}^{-1}\Big(\frac{A-1+\chi}{A+1-\chi}\Big) = \mathrm{cn}^{-1}\Big(\frac{A-1+(x/r)^2}{A+1-(x/r)^2}\Big), \quad u \in [-\beta,\, \beta] \tag{66}$$

and

$$\beta = \mathrm{cn}^{-1}\Big(\frac{A-1}{A+1}\Big).$$

For additional details of the reduction process, we refer the reader to the Handbook by Byrd and Friedman [1, Formulas (243.07) and (341.53)].

On returning back to the variable x in (65) we obtain the first explicit representation of the profile curves (upper right parts) of the surfaces of the third class

$$z_3(x) = \frac{r}{2\sqrt{A}}\Big(\big(\frac{2}{\nu-1} - A\big)F(\varphi, k_3) + 2A\big(E(\varphi, k_3) - \frac{\sin\varphi\Delta(\varphi)}{1+\cos\varphi}\big)\Big) \tag{67}$$

$$\varphi := \varphi(x) = \arccos\Big(\frac{A-1+(x/r)^2}{A+1-(x/r)^2}\Big), \qquad x \in [0, r]$$

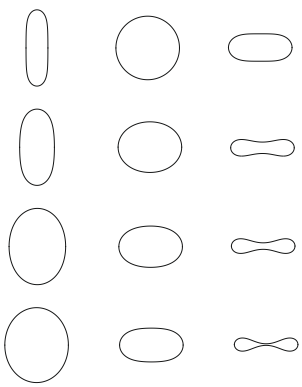

Figure 16. Prolate, oblate and biconcave profiles.

where the elliptic modulus k_3 and A are given by (63) and the roots σ_3 and τ_3 are calculated by (28) for the values of the parameter ν in the interval $(1, 9)$. Let us now introduce a new parameter

$$u = \arcsin\sqrt{\chi} = \arcsin\Big(\frac{x}{r}\Big), \quad u \in [-\frac{\pi}{2}, \frac{\pi}{2}] \tag{68}$$

which, as it is clearly seen from the commutative diagram in Fig. 15, should not be confused with the parameter u used in equations (62) – (65) where it is defined by the formulas (66).

The profiles in Fig. 16 are (from above): in the first column $\nu = 0.01,\ 0.1,\ 0.5$ and 0.7, in the second

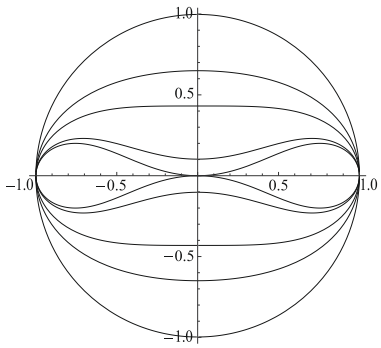

Figure 17. Some plots of the third class for $\nu = 1$, 2, 3, 5 and $\nu = 5.6582$ (from outside to inside).

column $\nu = 1$, 1.5, 2 and 2.5, and in the third column $\nu = 3$, 4.5, 5 and 5.5. Thus, we have two choices for the parameter u, given by formulas (66) and (68), in which u has different relationships with the variable χ (respectively x). The corresponding canonical representations of the surfaces of the third class, i.e., of the surfaces obtained for $\nu \in (1, 9)$, are given either by the set of equations

$$z_3(u)=r\sqrt{\frac{2\sqrt{\nu}}{\nu-1}}\left(\frac{1-\sqrt{\nu}}{2\sqrt{\nu}}F(\varphi,k_3)+E(\varphi,k_3)-\frac{\sin\varphi(u)\Delta(\varphi)}{1+\cos\varphi}\right)$$

$$\varphi:=\varphi(u)=\arccos\Big(\frac{2\sqrt{\nu}-(\nu-1)\cos^2 u}{2\sqrt{\nu}+(\nu-1)\cos^2 u}\Big),\quad k_3=\frac{\sqrt{(1+\sqrt{\nu})(3+\sqrt{\nu})}}{2\sqrt{2}\,\sqrt[4]{\nu}} \tag{69}$$

$$x(u,v)=r\sin u\cos v,\quad y(u,v)=r\sin u\sin v,\quad z(u,v)=z_3(u),\quad u\in[-\frac{\pi}{2},\frac{\pi}{2}]$$

or by another set which involve the parameter u, running however in a different range of values, i.e.,

$$z_3(u)=r\sqrt{\frac{2\sqrt{\nu}}{\nu-1}}\left(\frac{1-\sqrt{\nu}}{2\sqrt{\nu}}\,u+E(\mathrm{am}\,u,k_3)-\frac{\mathrm{sn}\,u\,\mathrm{dn}\,u}{1+\mathrm{cn}\,u}\right),\quad u\in[-\beta,\,\beta]$$

$$x_3(u)=r\sqrt{1-\frac{2\sqrt{\nu}}{\nu-1}\cdot\frac{1-\mathrm{cn}\,u}{1+\mathrm{cn}\,u}},\qquad \beta=\mathrm{cn}^{-1}\Big(\frac{2\sqrt{\nu}-\nu+1}{2\sqrt{\nu}+\nu-1}\Big) \tag{70}$$

$$x(u,v)=x_3(u)\cos v,\quad y(u,v)=x_3(u)\sin v,\quad z(u,v)=z_3(u),\quad v\in[0,2\,\pi]$$

where k_3 is defined in (69) and cn^{-1} is the inverse of the Jacobian cosine function. Note also that the angular parameter v runs over the same range in both parameterizations. For the parameterization (69), in the indicated interval of the parameter

u, only that part of the surface $\mathcal{S}$ which is over the XOY-plane (the upper half part) is obtained. The profile curve in the parameterization (69) is traced clockwise while for the parameterization (70) it is traced counterclockwise (see Fig. 17 and Fig. 18).

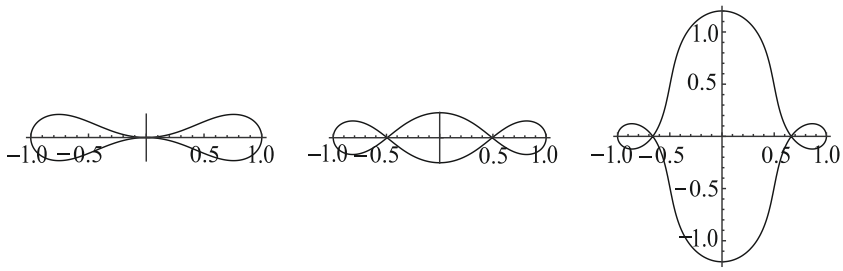

Figure 18. Some plots of the third class with $\nu = 5.6582$, 7 and 8.9 (from left to right).

Finally, the degenerated case $\nu \equiv 9$ is presented in Fig. 19 shown below.

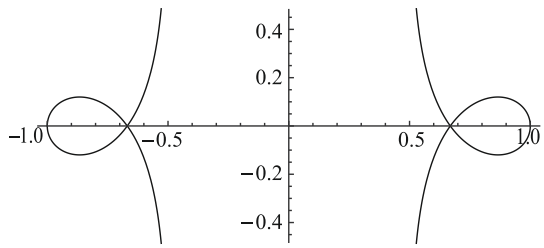

Figure 19. Plot of the degenerated case $\nu \equiv 9$ drawn by formula (19).

7. Shapes of the Fourth Class $\mathcal{S}^{\mathrm{IV}}(\nu)$

The shapes of the fourth class (for $\nu \in (9, +\infty)$, cf. Fig. 6) are open surfaces with self intersection lying inside the cylinder $\nu = 0$. According to equations (15) – (16) their profile curves (upper right parts) are given by the formula

$$z_4(\chi) = \frac{r}{2(\nu-1)} \int_{\chi}^{1} \frac{((\nu-1)t - \nu + 3)\mathrm{d}t}{\sqrt{(1-t)(t-\sigma_4)(t-\tau_4)}}, \quad \chi = \frac{x^2}{r^2}, \quad x \in [0,\, r]. \qquad (71)$$

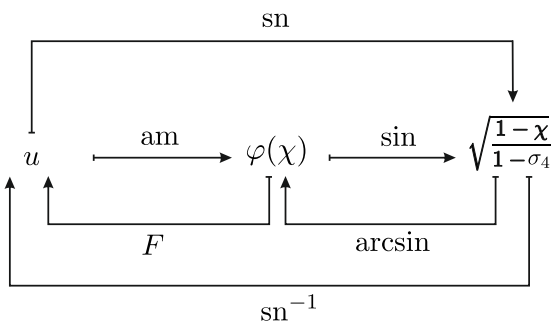

Figure 20. Commutative diagram illustrating the "inversion procedure" for the canonization of the elliptic integral (71).

where the roots σ_4 and τ_4 of the polynomial $P(t)$, calculated by the equations (28) for $\nu \in (9, \infty)$, are such that the following inequalities hold (compare with the fourth item (29) and (31))

$$0 < \tau_4 < \sigma_4 < t < 1, \qquad 0 < \tau_4 < \sigma_4 \leq \chi \leq 1. \tag{72}$$

In the limiting case $\nu = +\infty$ the surfaces degenerate to a circle of radius r. The reduction of the above elliptic integral goes through the "inversion procedure", as illustrated by the commutative diagram in Fig. 20, on writing

$$t = 1 - (1 - \sigma_4)\mathrm{sn}^2(\tilde{u}, k_4), \qquad \chi = 1 - (1 - \sigma_4)\mathrm{sn}^2(u, k_4) \tag{73}$$

where

$$u = F(\varphi(\chi), k_4), \qquad \varphi(\chi) = \arcsin\sqrt{\frac{1-\chi}{1-\sigma_4}}, \qquad k_4 = \sqrt{\frac{1-\sigma_4}{1-\tau_4}}. \tag{74}$$

By substituting and integrating in succession the profile curve in (71) is reduced to a representation involving only normal elliptic integrals of the first and the second kind (cf. [1, Formula (236.20)])

$$
\begin{aligned}
z_4(\chi) &= \frac{r}{\nu-1}\int\limits_0^u \frac{\big(2-(\nu-1)(1-\sigma_4)\mathrm{sn}^2\tilde{u}\big)\,\mathrm{dn}\,\tilde{u}\,\mathrm{d}\tilde{u}}{\sqrt{1-\tau_4-(1-\sigma_4)\mathrm{sn}^2\tilde{u}}} \\
&= \frac{r}{(\nu-1)\sqrt{1-\tau_4}}\int\limits_0^u \frac{\big(2-(\nu-1)(1-\sigma_4)\mathrm{sn}^2\tilde{u}\big)\,\mathrm{dn}\,\tilde{u}\,\mathrm{d}\tilde{u}}{\sqrt{1-k_4^2\,\mathrm{sn}^2\tilde{u}}} \\
&= \frac{r}{\sqrt{1-\tau_4}}\int\limits_0^u \left(\frac{2}{\nu-1}-(1-\sigma_4)\mathrm{sn}^2\tilde{u}\right)\mathrm{d}\tilde{u} \qquad (75)\\
&= \frac{r}{\sqrt{1-\tau_4}}\left(\frac{2}{\nu-1}\int\limits_0^u \mathrm{d}\tilde{u}-\frac{1-\sigma_4}{k_4^2}\Big(\int\limits_0^u \mathrm{d}\tilde{u}-\int\limits_0^u \mathrm{dn}^2\tilde{u}\,\mathrm{d}\tilde{u}\Big)\right) \\
&= \frac{r}{\sqrt{1-\tau_4}}\Big(\Big(\tau_4-\frac{\nu-3}{\nu-1}\Big)F(\varphi(\chi),k_4)+(1-\tau_4)E(\varphi(\chi),k_4)\Big).
\end{aligned}
$$

In the above chain of equalities we have made use of the formulas (25) – (27), and as well as, the formula for the derivative of the Jacobian sine elliptic function (refer to Section 3).

On returning back to the variable x in the last line of (75) we arrive at our first explicit parameterization of the profile curves of the surfaces of the fourth class in Monge representation

$$
\begin{aligned}
z_4(x) &= \frac{r}{\sqrt{1-\tau_4}}\Big(\Big(\tau_4-\frac{\nu-3}{\nu-1}\Big)F(\varphi(x),k_4)+(1-\tau_4)E(\varphi(x),k_4)\Big) \qquad (76)\\
\varphi(x) &= \arcsin\sqrt{\frac{1-(x/r)^2}{1-\sigma_4}}, \qquad k_4=\sqrt{\frac{1-\sigma_4}{1-\tau_4}}, \qquad x\in[r\sqrt{\sigma_4},r]
\end{aligned}
$$

where σ_4 and τ_4 are calculated by (28) for each one of the surfaces with a parameter $\nu\in(9,+\infty)$. Note that the above formula describes only the lower right part of the profile curve. The whole curve is obtained by two consecutively applied reflections with respect to the coordinate axes OX and OZ (cf. Fig. 3).

Now we are going to give two canonical representations of the surfaces of the fourth class obtained from (76) by referring to the roots of the polynomial $P(t)$

as functions of ν and substituting for χ with a new parameter u, defined in two different ways, either by the equations

$$u = \arcsin\sqrt{\chi} = \arcsin\left(\frac{x}{r}\right), \qquad u \in \left[\arcsin\sqrt{\sigma_4},\ \frac{\pi}{2}\right] \tag{77}$$

or by the equations

$$u = \mathrm{sn}^{-1}\Big(\sqrt{\frac{1-\chi}{1-\sigma_4}}\Big) = \mathrm{sn}^{-1}\Big(\sqrt{\frac{1-(x/r)^2}{1-\sigma_4}}\Big), \quad u\in[-K(k_4),\ K(k_4)]\,. \tag{78}$$

We have two choices for the parameter u, i.e., (77) and (78) with different ranges and relationships with the variable χ (respectively the coordinate x). Their notation should not create however confusion in respective parameterizations of the profile curves. The commutative diagram in Fig. 20 may serve to elucidate the meaning of the second choice.

As a result the corresponding canonical representations of the surfaces of the fourth class, i.e., of the surfaces obtained for $\nu \in (9, +\infty)$, are given either by the set of equations

$$\begin{gathered}
z_4(u)=r\Big(\frac{2\delta-1}{2\lambda_4}\,F(\varphi(u),k_4)+\lambda_4 E(\varphi(u),k_4)\Big), \qquad k_4=\frac{\mu_4}{\lambda_4}\\
\lambda_4=\sqrt{\frac{(1-2\delta)\nu+2\delta+3}{2(\nu-1)}}, \qquad \mu_4=\sqrt{\frac{(1+2\delta)\nu-2\delta+3}{2(\nu-1)}}\\
\varphi(u)=\arcsin\left(\frac{\cos u}{\mu_4}\right), \qquad \delta=\frac{\sqrt{(\nu-1)(\nu-9)}}{2(1-\nu)}, \qquad \beta=\arcsin\sqrt{1-\mu_4^2}
\end{gathered} \tag{79}$$

$$x(u,v)=r\,\mathrm{sin}u\,\cos v, \quad y(u,v)=r\,\mathrm{sin}u\,\sin v, \quad z(u,v)=z_4(u), \quad u\in\Big[\beta,\ \frac{\pi}{2}\Big]$$

or by another set of equations in which the parameter u appears again, but this time with a different range, i.e.,

$$\begin{gathered}
x_4(u)\,=\,r\sqrt{1-\mu_4^2\,\mathrm{sn}^2\,u}, \qquad z_4(u)=r\Big(\frac{2\delta-1}{2\lambda_4}\,u+\lambda_4 E(\mathrm{am}\,u,k_4)\Big)\\
x(u,v)\,=\,x_4(u)\cos v, \quad y(u,v)=x_4(u)\sin v, \qquad z(u,v)=z_4(u)
\end{gathered} \tag{80}$$

where λ_4, μ_4 and the modulus k_4 are defined in (79), $u\in[-K(k_4),\ K(k_4)]$ and $v\in[0,2\,\pi]$. Notice that the second parameter v, which is the same for both parameterizations, coincides with the angular coordinate of the meridians.

Figure 21. Some plots of the fourth class shapes generated with $\nu = 9,\ 10$ and 13 (from left to right).

All surfaces of the fourth class are open surfaces placed inside the cylinder $\nu = 0$ and have a circle of self intersection (see Fig. 21).

8. Geometry: Geodesics

Having whatever explicit parameterization of the surface $\mathcal{S}$ one can compute the coefficients E, F, G of its first, respectively L, M and N of its second fundamental form either by hand or with the help of some Computer Algebra System like `Mathematica` or *Maple*. The description of the *Maple* worksheet for the case under consideration can be found in [13] and the result of these computations is

$$\begin{aligned} E &= \frac{1}{1-(\tilde{a}x^3+\tilde{c}x)^2}, \qquad F = 0, \qquad G = x^2 \\ L &= \frac{3\tilde{a}x^2+\tilde{c}}{1-(\tilde{a}x^3+\tilde{c}x)^2}, \qquad M = 0, \qquad N = x^2(\tilde{a}x^2+\tilde{c}). \end{aligned} \tag{81}$$

The knowledge of the fundamental forms open the possibility to study more deeply the properties of the surface, e.g. to find out its geodesic curves. Finding the geodesics on surfaces has a long history in geometry because they are intimately tied up with, for instance, the symmetry properties of the surface. In physics, geodesics are trajectories of freely moving particles subject only to the constraint forces keeping them on the surface. Thus, geodesics often help us to understand geometrical and physical qualities of the surface which usually is the configurational space of some mechanical system. The geodesic equations present a complicated system of second order differential equations which rarely can be integrated analytically. In the case of surfaces of revolution this problem is reduced to the evaluation of the integral

$$v(u) = \pm \int^u \frac{h\sqrt{E}}{\sqrt{G}\,\sqrt{G-h^2}}\,\mathrm{d}\tilde{u}, \qquad h \in (0,\,1). \tag{82}$$

As we are dealing with four classes of surfaces this means that we have to evaluate at least four integrals which will increase significantly the volume of the paper.

That is why we choose to do this for the second class of prolate spheroids and accordingly the integral becomes

$$v(u) = \pm\frac{h}{1-\nu}\int^{u}\frac{\mathrm{d}t}{t\sqrt{(1-t)(t^2-\frac{\nu^2-6\nu+5}{(1-\nu)^2}\,t+\frac{4}{(1-\nu)^2})(t-h^2)}}. \tag{83}$$

In order to determine the function $v(u)$ let us denote the respective roots of the polynomial under the radical in (83) as $\alpha_1 \equiv \tau_2 > \alpha_2 \equiv \sigma_2 > \alpha_3 \equiv 1 > \alpha_4 \equiv h^2$ and consider the integral

$$\tilde{I} = \int\frac{\mathrm{d}t}{\sqrt{(t-\alpha_1)(t-\alpha_2)(\alpha_3-t)(t-\alpha_4)}}. \tag{84}$$

Next, let us exchange the variable t for ξ by making use of the formula

$$t := \frac{\alpha_1(\alpha_3-\alpha_4)\xi^2+\alpha_1\alpha_4-\alpha_3\alpha_4}{(\alpha_3-\alpha_4)\xi^2+\alpha_1-\alpha_3}. \tag{85}$$

In this way the integral (84) is transformed into its almost canonical form, i.e.,

$$\tilde{I} = \int\frac{2\mathrm{d}\xi}{\sqrt{(1-\xi^2)\big((\alpha_1-\alpha_3)(\alpha_2-\alpha_4)-(\alpha_1-\alpha_2)(\alpha_3-\alpha_4)\xi^2\big)}} \tag{86}$$

which suggest also to introduce additionally the notation

$$m := \sqrt{(\alpha_1-\alpha_3)(\alpha_2-\alpha_4)}, \qquad k = \sqrt{\frac{(\alpha_1-\alpha_2)(\alpha_3-\alpha_4)}{(\alpha_1-\alpha_3)(\alpha_2-\alpha_4)}} \tag{87}$$

and a quick check proves that $k^2 < 1$. Doing so we end up with the expression

$$\tilde{I} = \frac{2}{m}\int\frac{\mathrm{d}\xi}{\sqrt{(1-\xi^2)(1-k^2\xi^2)}} \tag{88}$$

which makes obvious the fact that the integral on the right can be inverted via the Jacobian elliptic function $\mathrm{sn}(\tilde{u},k)$, i.e., the replacement of ξ by $\mathrm{sn}(\tilde{u},k)$ produces

$$\tilde{I} = \frac{2}{m}\tilde{u}. \tag{89}$$

Combining all above we can conclude that the sought function $v(u)$ can be determined explicitly by the evaluation of the elliptic integral of the third kind in the form

$$\int\frac{\alpha+\beta\,\mathrm{sn}^2(\tilde{u},k)}{\lambda+\mu\,\mathrm{sn}^2(\tilde{u},k)}\mathrm{d}\tilde{u}. \tag{90}$$

This will be not detailed here as the final result depends crucially on the fine relationships between the roots α_i, $i = 1, ..., 4$. The interested reader however can find the complete description of the procedure in any concrete case in the book by Lawden [6, page 68] . Alternatively, a modification of the above integral is considered in Whittaker & Watson [24, Ch. XXII, page 522] where one can find the useful formula

$$\int \frac{\tilde{\alpha} + \tilde{\beta}\,\mathrm{sn}^2(\tilde{u}, k)}{1 + \tilde{\nu}\,\mathrm{sn}^2(\tilde{u}, k)} \mathrm{d}\tilde{u} = \tilde{\alpha}\, u + (\tilde{\beta} - \tilde{\alpha}\,\tilde{\nu}) \int \frac{\mathrm{sn}^2(\tilde{u}, k)}{1 + \tilde{\nu}\,\mathrm{sn}^2(\tilde{u}, k)} \mathrm{d}\tilde{u}. \qquad (91)$$

in which $\tilde{\alpha}, \tilde{\beta}, \tilde{\nu}$ are real parameters which can be obtained directly from the original ones α, β, λ and μ in (90).

9. Concluding Remarks

We have seen that starting from the first principles the problem of finding the equilibrium of the system of two co-rotating with a constant angular velocity immiscible fluids is equivalent with that of finding an axially symmetric surface with a prescribed mean curvature depending on two real parameters. In this formulation there exists also a hidden parameter - the integration constant C in equations (8). If this constant is fixed to zero one ends with a problem about a two parametric family of axially symmetric linear Weingarten surfaces which mean curvature as a function of the distance $\mathcal{R}$ from the axis of revolution is given by the function

$$H = \frac{\nu - 1}{r^3}\mathcal{R}^2 + \frac{3 - \nu}{2r}$$

in which the two characteristic parameters r and ν account respectively for the size and the shape of the surfaces. We have succeeded to distinguish four classes of shapes which are presented by their explicit parameterizations in terms of elliptic integrals and Jacobian elliptic functions. At both limits $\nu = -\infty$ and $\nu = +\infty$ the surfaces degenerate to a circle $\mathcal{C}_r$, where r is the radius of the circle.
Assuming solely axisymmetric configurations the drop evolves with the change of the parameter ν in the range $\nu \in [-\infty, +\infty]$ starting from $\mathcal{C}_r$, passing consecutively through the right circular cylinder $\nu = 0$, the sphere $\nu = 1$, then the linear Weingarten surface $LW(2) \equiv \mathcal{S}^{\mathrm{III}}(3)$, and finally returning back to the circle $\mathcal{C}_r$. In more details the sequence of transformed shapes obtained under the change of the parameter ν are presented in Table 4.
Let us mention also that the equilibrium shapes of the rotating spheroids and drops have been reviewed by Wang [23] but without any details about their analytical description.

It was one of the principle aims of the present work to fill this gap and to initiate the complete classification of all shapes. Another one was to study their geometry, i.e., line elements, surfaces areas, volumes and geodesics that will be explored in the future.

Acknowledgements

The authors are thankful to Dr Mariana Hadzhilazova and Venelin Chernogorov for their help in preparation of this article.

Table 4. The sequence of shapes obtained by the change of the parameter ν.

class	ν	Shapes
$\mathcal{C}_r$	$-\infty$	circle of radius r
$S^I(\nu)$	$(-\infty, 0)$	open toroids (Fig. 11)
	0	right circular cylinder
$S^{II}(\nu)$	$(0, 1)$	closed prolate spheroids (Fig. 14) and (Fig. 16)
	1	sphere
$S^{III}(\nu)$	$(1, 3)$	closed oblate spheroids (Fig. 16)
	3	$LW(2)$ - (Fig. 16) and (Fig. 17)
	$(3, 5.6582)$	closed biconcave discoids (Fig. 16) and (Fig. 17)
	5.6582	biconcave discoid with a contact point (Fig. 17) and (Fig. 18)
	$(5.6582, 9)$	closed surfaces with self intersection (Fig. 18)
	9	open surface with self intersection parameterized via elementary functions (Fig. 19)
$S^{IV}(\nu)$	$(9, +\infty)$	open surfaces with self intersection (Fig. 21)
$\mathcal{C}_r$	$+\infty$	circle of radius r

References

[1] Byrd P. and Friedman M., *Handbook of Elliptic Integrals for Engineers and Scientists*, 2nd Edn, Springer, New York 1971.

[2] Castro I. and Castro-Infantes I., *Plane Curves with Curvature Depending on the Distance to a Line*, Diff. Geom. Appl. **44** (2016) 77-97.

[3] Castro I., Castro-Infantes I. and Castro-Infantes J., *New Plane Curves with Curvature Depending on Distance from the Origin*, Mediterr. J. Math. **14** (2017) 108.

[4] Chandrasekhar S., *The Stability of a Rotating Liquid Drop*, Proc. R. Soc. Lond. A **286** (1965) 1-26.

[5] Hynd R. and McCuan J., *On Toroidal Rotating Drops*, Pacific J. Math. **224** (2006) 279–289.

[6] Lawden D., *Elliptic Functions and Applications*, Springer, New York 1989.

[7] Lopez R., *On Linear Weingarten Surfaces*, Int. J. Math. **19** (2008) 439-448.

[8] Lopez R., *Special Weingarten Surfaces Foliated by Circles*, Monatsh Math **154** (2008) 289-302.

[9] Mladenov I., *On the Geometry of the Mylar Balloon*, C. R. Bulg. Acad. Sci. **54** (2001) 39-44.

[10] Mladenov I. and Hadzhilazova M., *The Many Faces of Elastica*, Springer, Cham 2017.

[11] Mladenov I. and Oprea J., *The Mylar Ballon*: *New Viewpoints and Generalizations*, Geom. Integrability & Quantization **8** (2007) 246-263.

[12] Mladenov I. and Oprea J., *On Some Deformations of the Mylar Balloon*, Publ. de la RSME **11** (2007) 308-315.

[13] Mladenov I. and Oprea J., *On the Geometry of the Rotating Liquid Drop*, Math. Comput. Stimulat. **127** (2016) 194-202.

[14] Nurse A., Coriell S. and McFadden G., *On the Stability of Rotating Drops*, J. Res. Natl. Inst. Stand. Technol. **120** (2015) 74-101.

[15] Oprea J., *Differential Geometry and Its Applications*, 2nd Edn, Prentice Hall, Upper Saddle River 2003.

[16] Palmer B. and Perdomo O., *Equilibrium Shapes of Cylindrical Rotating Liquid Drops*, Bull Braz Math Soc **46** (2015) 515-561.

[17] Pampano A., *Planar p-Elasticae and Rotational Linear Weingarten Surfaces*, Geom. Integrability & Quantization **20** (2019) 227-238.

[18] Plateau J., *Experimental and Theoretical Researches on the Figures of Equilibrium of a Liquid Mass Withdrawn From the Action of Gravity*, Phil. Mag. **14** (1857) 1-22.

[19] Pulov V., Hadzhilazova M. and Mladenov I., *On a Class of Linear Weingarten Surfaces*, Geom. Integrability & Quantization **19** (2018) 168–187.

[20] Pulov V., Hadzhilazova M. and Mladenov I., *Deformations Without Bending*: *Explicit Examples*, Geom. Integrability & Quantization **20** (2019) 246–254.

[21] Rayleigh, Lord, *The Equilibrium of Revolving Liquid Under Capillary Force*, Phil. Mag. **28** (1914) 161-170.

[22] Vonnegut B., *Rotating Bubble Method for the Determination of Surface and Interfacial Tensions*, Rev. Sci. Instr. **13** (1942) 6-9.

[23] Wang T., *Equilibrium Shapes of Rotating Spheroids and Drop Shape Oscillations*, Adv. Appl. Mech. **26** (1988) 1-62.

[24] Whittaker E. and Watson G., *A Course of Modern Analysis*, Cambridge Univ. Press, Cambridge 1962.

Vladimir I. Pulov
Department of Physics
Technical University of Varna
Varna 9010, Bulgaria
E-mail address: vpulov@hotmail.com

Ivaïlo M. Mladenov
Institute of Biophysics
and Biomedical Engineering
Bulgarian Academy of Sciences
Acad. G. Bonchev Str., Bl. 21
1113 Sofia, BULGARIA
E-mail address: mladenov@bio21.bas.bg